Int. J. Heat Mass Transfer. Vol. 31, No. 1, pp. 167–176, 1988
Printed in Great Britain

0017–9310/88 $3.00+0.00

A sublayer description for the air friction acting on thin filaments during melt spinning

C. BOS
Enka bv Research Institute Arnhem, Velperweg 76, 6824 BM Arnhem, Holland

(*Received* 18 *May* 1987 *and in final form* 31 *May* 1987)

Abstract—The air friction on small diameter filaments is explained from a sublayer description of the air flow along the filament surface. The air friction on the filaments is expressed by the dimensionless Bingham number, *Bm*, as

$$Bm = P(\ln(1+1.29Re_x^{1/3}\,Re_R^{-1}))^{-1}$$

where P is a measure of the relative velocity drop across the sublayer. Results calculated from this formula correspond with many experimental results and with a turbulent boundary layer calculation. This formula also explains experimental results for heat transfer obtained with hot wire anemometers and with cylinders in longitudinal flow.

1. INTRODUCTION

THE MELT spinning of synthetic filament yarns is an important production process, which has been used for 50 years. A large amount of the literature published on this subject has partly been reviewed by Ziabicki [1]. In the melt spinning process, shown in Fig. 1, a suitable polymer is melted and forced through small spinneret holes to enter the air, where it is solidified by cooling. The solidified polymer flowing from a hole is called a filament. A spinneret plate usually has more holes. All filaments formed at the same spinneret plate form a filament bundle, which is usually called a yarn. After solidification the yarn is provided with a spinning oil and transported to the drawing or winding section. Transport takes place by means of a driven roller called a godet, combined with an idler roller. The godet with idler pulls on the yarn at a fixed speed v. The elongation in the zone where the polymer is hot and deformable, is determined by the polymer speed in the spinneret hole and the velocity of the godet. As the melt spinning process is controlled by the yarn cooling and the air friction in the elongation zone, a thorough understanding of the transfer processes of heat and momentum will be necessary to improve process knowledge. An investigation into the behaviour of the boundary layer has contributed to a better understanding of the transfer processes. For making a reliable computer simulation of the melt spinning process, an accurate description of the transfer processes will be essential.

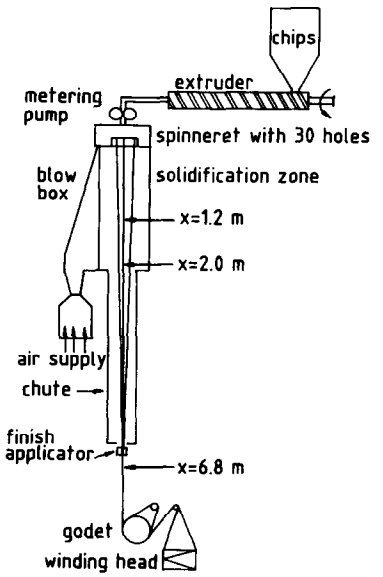

FIG. 1. Set-up of a melt spinning machine. The yarn force is measured at x = 1.2, 2.0 and 6.8 m from the orifice.

The air surrounding the filaments counteracts the movement of the filament by air friction, leading to an increase of pull in the yarn. The air friction on filaments has been the subject of investigation of various authors (see p. 182 of ref. [1]). Gould and Smith [2] improved the experimental techniques and obtained reliable results, which can be explained from the turbulent behaviour of the boundary layer. Theoretical expressions for air friction have been published by Glicksman [3] and Mayer [4]. The procedure used by them for the numerical calculation of the air friction on filaments was complex and laborious and did not result in analytical expressions. In this paper an analytical expression for air friction is derived. This expression improves the physical insight into the phenomenon of air friction and simplifies the model calculations for the melt spinning process.

In our experiments we have investigated the influence of various factors on the force build-up of spinning filaments. The experimental results are explained by using a sublayer description for the air flow along the filament. In general, with flow around large

NOMENCLATURE

a_a	molecular thermal diffusivity of air [$m^2 s^{-1}$]
$a_1, a_2, A, B, \alpha, \beta, b_1, b_2$	coefficients for numerical fit
C_f	coefficient of air drag
F_r	force on a single filament [N]
F_g, F_{ad}	force contribution due to gravity and air drag, respectively [N]
g	gravitational constant, 9.81 m s^{-2}
P	relative velocity drop across the sublayer, equation (15)
r	distance from the cylinder axis [m]
R	radius of the cylinder or the filament [m]
t	time [s]
T_a	temperature of air [K]
v, v_a	speed in x-direction of polymer and air, respectively [m s^{-1}]
v_{a0}	air speed v_a on transition of sublayer and boundary layer [m s^{-1}]
x	distance from orifice of spinning filament in axial direction [m].

Greek symbols

α^*	coefficient of heat transfer from filament to air [$W m^{-2} K^{-1}$]
δ	sublayer thickness [m]
η_a	dynamic viscosity of air [Pa s]
λ_a	coefficient of heat conductance of air [$W m^{-1} K^{-1}$]
ν_a	kinematic viscosity of air, η_a/ρ_a [$m^2 s^{-1}$]
ρ, ρ_a	density of polymer and air, respectively
τ_w	shear tension in the air stream at the wall [Pa]
ϕ_m	mass flow or output per spinneret orifice [kg s^{-1}].

Dimensionless numbers

Bm	Bingham number for transfer of momentum, $\tau_w R/\eta_a v$
Nu	Nusselt number for transfer of heat, $\alpha^* R/\lambda_a$
Pr	Prandtl number, ν_a/a_a
Re_R	radius Reynolds number, vR/ν_a
Re_x	length Reynolds number, vx/ν_a

objects, the sublayer concept is used only as a boundary condition for turbulent boundary layer calculations because the sublayer is very thin and of minor importance for normal flow behaviour. Since the filaments are also thin, the sublayer thickness will have the same dimensions as the filament diameter. As a result the sublayer behaviour becomes decisive for the description of the air friction. For thin filaments it will be shown that the transfer of both heat and momentum can be fully described by analysing the behaviour of the sublayer.

2. EXPERIMENTAL SET-UP FOR THE DETERMINATION OF THE AIR FRICTION

Experiments have been carried out on a spinning machine as shown in Fig. 1. Polyethylene terephthalate chips are melted in an extruder and fed to a spinning pump, which meters the polymer flow to the spinneret containing 30 orifices. The fluid polymer jets leaving the orifices first travel through a short hot air zone and are subsequently cooled in a blow box by a cold air stream transverse to the filaments. Under the blow box, having a length of 2 m, a 4 m long pipe is positioned which operates as a chute for the spinning filament bundle. Below this pipe the filaments are assembled on a spin finish applicator and fed to the first godet determining the spinning speed.

2.1. *Measurements*

A device for measuring the yarn forces is fitted in the spinning line at three distances from the spinneret, namely 1.2, 2.0 and 6.8 m. The force acting on all 30 filaments is measured collectively. It has been shown experimentally that the force is proportional to the number of filaments in the bundle when varying the number of orifices in the spinneret. The total force on all filaments is called yarn force. The device for force measurements consists of an airborne idler roller secured to the end of a spring leaf. The bending momentum of the roller, caused by the yarn force, is taken over by strain gauges, amplified and recorded. By using the airborne roller the friction on the yarn due to the measurements will be minimal. The influence of the measurements on the running of the process can be neglected.

In the experimental set-up the influence of various factors on the force build-up has been investigated: distance from the orifice, mass flow per spinneret hole, spinning speed and the number of filaments per bundle. As force measurements on the spinning yarn can only be performed if the filaments have solidified, it has not been possible, at high outputs per hole, to carry out measurements at a distance of 1.2 m from the spinneret.

For the determination of the output per spinneret hole, the polymer flow is collected under the spinneret during a certain time. By weighing the collected amount of polymer the output is known.

2.2. *Processing of experimental data*

The spinning filament forms a stream tube. At increasing spinning speed v, the filament radius R decreases if the output per hole stays the same according to

$$\phi_m = \pi R^2 \rho v. \tag{1}$$

This relationship, which is characteristic of melt spinning is frequently used in this paper.

The increase in force (F_r) on the solidified filament comes from the gravity force (F_g) and the air friction (F_{ad}) because inertia forces can be neglected in this zone. The following balance of forces holds:

$$\frac{d}{dx}F_r + \frac{d}{dx}F_g = \frac{d}{dx}F_{ad}. \tag{2}$$

The influence of gravity can be expressed by

$$\frac{d}{dx}F_g = \rho g \pi R^2. \tag{3}$$

Elimination of R from these equations, using equation (1), yields

$$\frac{d}{dx}F_r = \frac{d}{dx}F_{ad} - \frac{\phi_m g}{v}. \tag{4}$$

The air friction can be characterized by a dimensionless number for transfer of momentum: the Bingham number, Bm. This is defined by the ratio of the actual measured wall shearing stress $\tau_w = (dF_{ad}/dx)/(2\pi R)$ and the viscous shearing stress $(\eta_a v/R)$ according to

$$Bm = \frac{\tau_w R}{\eta_a v} = \frac{1}{2\pi\eta_a v}\frac{d}{dx}F_{ad}. \tag{5}$$

In the literature use is often made of the local coefficient of friction C_f which is related to the Bingham number, Bm, and the Reynolds number, Re_R

$$Bm = \tfrac{1}{2}C_f Re_R. \tag{6}$$

The Bingham number can now be calculated from the force measurements by eliminating F_{ad} from equations (4) and (5), which leads to

$$Bm = \frac{1}{2\pi\eta_a v}\left(\frac{d}{dx}F_r + \frac{\phi_m g}{v}\right). \tag{7}$$

For the value of the air viscosity use is made of the following well-known approximation:

$$\eta_a = (3.35 + 0.05T_a)\times 10^{-6}. \tag{8}$$

3. EXPERIMENTAL RESULTS

3.1. *Variations in yarn force*

The yarn force is found to show a statistical variation with a peak-to-peak value of about 20% of the average value. The mean yarn force is determined by averaging the yarn force for several minutes. The resulting value is used for analysing the measurements. The accuracy of the force measurements is estimated to be 5% if reproduced on the same day. Repeating the experiments at intervals of a few days may reveal differences up to 10% of the value of this average yarn force.

By averaging over a large number of experimental results, acceptable correlations are found. The scatter of the individual points may be explained from the inherent unstable character of the turbulent air layer next to the sublayer of the spinning filament.

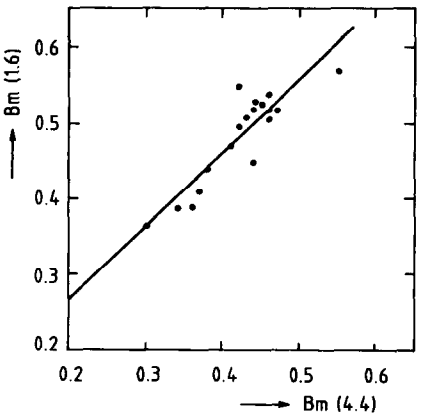

FIG. 2. Influence of distance from the spinneret hole on Bingham number.

3.2. *Distance from the spinneret hole*

The yarn force is dependent on the distance to the spinneret. From the measured yarn forces the Bingham number is obtained with the aid of equation (7). $Bm(1.6)$ is the value of Bm in the blow box at a distance of 1.6 m from the spinneret. $Bm(1.6)$ is calculated from the forces measured at 1.2 and 2.0 m from the hole. $Bm(4.4)$ is the value of Bm in the middle of the chute. $Bm(4.4)$ is computed from the forces measured at a distance of 2.0 and 6.8 m from the spinneret. In Fig. 2 the values of $Bm(1.6)$ and $Bm(4.4)$ are shown together with the linear regression of these data

$$Bm(1.6) = 0.062 + Bm(4.4). \tag{9}$$

It is clear that the air friction decreases with increasing distance from the orifice. This effect is important for the theoretical explanation given below.

3.3. *Spinning speed and output per spinneret hole*

A higher spinning speed gives rise to an increase in yarn force. The influence of the spinning speed on the value of Bm is far smaller because the yarn force is divided by the yarn speed according to equation (7). In Table 1 the data of $Bm(4.4)$, calculated from the force measurements, are given for various settings of the spinning machine. The Bingham number and the air friction slightly increase with increasing output per hole and spinning speed. Regression of all data from Table 1 with a power-law relation yields the following equation with a correlation coefficient of 0.94:

$$Bm(4.4) = 3.2 v^{0.08}\phi_m^{0.22}. \tag{10}$$

4. THEORETICAL CONSIDERATIONS ON THE AIR FLOW ALONG A SPINNING FILAMENT

4.1. *General survey*

The behaviour of the air flow along a spinning filament can be divided into the following regimes:

Table 1. Experimental results for the air friction on a spinning yarn bundle

ϕ_m (10^{-5} kg s^{-1})	v (m s^{-1})	$Bm(4.4)$ measured	δ (μm) for $P = 0.8$	δ (μm) for $P = 1.0$	$Re_x/Re_R^{\frac{1}{2}}$
1.33	17	0.34	132	248	1382
1.33	30	0.33	107	205	1040
1.33	40	0.35	80	148	901
1.33	37	0.34	89	168	937
6.67	17	0.48	133	218	123
6.67	31	0.52	84	134	91
6.67	44	0.54	66	104	77
6.67	59	0.56	53	83	66
6.67	68	0.58	46	71	62
3.07	16	0.37	167	302	406
3.07	31	0.40	100	174	292
3.07	47	0.46	59	99	237
2.67	39	0.46	61	101	320
2.67	39	0.44	67	113	320
2.67	16	0.40	129	226	501
2.67	30	0.38	106	190	366
2.67	44	0.41	74	128	302
2.67	53	0.48	48	78	275
1.40	40	0.35	82	152	834
2.76	40	0.41	79	136	301
4.17	40	0.48	69	112	162
5.57	40	0.54	63	99	105
1.40	40	0.35	82	152	834

(a) the sublayer, i.e. the air layer very near to the surface where the flow behaviour is determined solely by the viscous behaviour of air;

(b) the boundary layer, i.e. the layer just outside the sublayer where viscous forces and inertia forces are of the same magnitude;

(c) the free fluid flow, i.e. the air flow outside the boundary layer where viscous forces have no influence.

For a spinning yarn the free fluid flow is determined by the shape and dimensions of the bundle, the spinning machine, the blow box, the settings of the machine and the air conditioning. A general description of the free fluid flow cannot be given.

Boundary layer descriptions are used in the literature to explain the force build-up and cooling of spinning filaments. Acierno *et al.* [6] and Glicksman [3] came to the conclusion that the laminar boundary layer calculation cannot be applied to spinning yarn. This is because the boundary layer of the spinning filament is not laminar but turbulent.

Sublayer descriptions, however, have never been used to explain the behaviour of spinning yarn, although the thermal and dynamical transfer of spinning filaments is strongly influenced by the sublayer flow. A sublayer description for spinning filaments will be developed here. The observed experimental behaviour of spinning filaments is used to quantify the sublayer behaviour.

4.2. *Axial-symmetrical turbulent boundary layer flow longitudinal to a long thin cylinder*

Sparrow *et al.* [7] computed the velocity profile for a flow longitudinal to a cylinder. Glicksman [3] used this method for calculating the heat transfer and the force build-up during the spinning of glass fibres. He found a relation between the drag coefficient and the radius Reynolds number, Re_R. This calculated result has been reproduced in Fig. 3, using equation (6) and Fig. 3 of ref. [3]. Unlike our results, Glicksman supposed that there was no influence of cylinder length on air drag for $Re_x > 10^5$.

Mayer [4] computed the force build-up on spinning filaments, starting from the general approximations for turbulent boundary layer flow as described by Walz [8]. Equations derived for the laminar boundary layer flow are used by Mayer and Walz for turbulent flow by application of experimental relations for wall shear stress and eddy viscosity (see, e.g. equations (3.111)–(3.114) in ref. [8]).

For the boundary condition they employed the experimentally found universal velocity profile for the wall region. This implies that the boundary of the turbulent flow is formed by the sublayer and not by the wall surface (Section 3.5.3 in ref. [8]). Using Walz's method, Mayer calculated the air drag and the heat transfer for a long thin cylinder of constant diameter. The result of his calculation is also reproduced in Fig. 3. Unlike Glicksman, Mayer predicted an influence of the cylinder length (Re_x) on the heat transfer.

For comparing the calculated results with the experimental results, our results and those of Gould and Smith are shown in Fig. 3.

The approximations of Glicksman and Mayer lead to different results for Bm and for the influence of Re_x. This difference stems from the difference in approximations used for calculating the turbulent boundary layer flow.

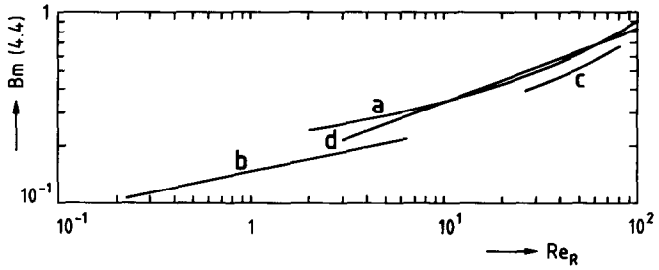

FIG. 3. Values of *Bm* following from turbulent boundary layer calculations (a, b) compared with experimental results (c, d): (a) Glicksman [3], Fig. 3; (b) Mayer [4], Fig. 6; *Bm* depends on Re_x; $(x/R) = 20.000$; (c) our results at $v = 40$ m s^{-1}; (d) results of Gould and Smith [2], Fig. 11.

These calculations have the following disadvantages:

(a) experimental relations are required for solving the equations; these relations are found in experiments on turbulent flow under comparable conditions;

(b) numerical solutions are only found for well-defined boundary conditions;

(c) the physical explanation of the processes determining thermal and dynamical transfer is missing.

4.3. *Visual investigation of the air flow in the sublayer*

The importance of the viscous sublayer for the heat transfer into turbulent shear flows was mentioned by Prandtl [9]. The sublayer concept has played only a qualitative role in the development of the boundary layer theory [10]. Einstein and Li [11] visualized the flow at the boundary and found an inherently unsteady sublayer which periodically builds up and disintegrates. For the turbulent flow along flat plates the sublayer has no laminar character. This flow character in the sublayer has been visualized by Kline *et al.* [12]. The movement of bubbles is followed photographically. Analysing their photographs Kline *et al.* observed the formation of low-speed streaks consisting of a lump of fluid which lifts up and bursts into ejection of the low momentum fluid into the fast moving outer region. Corino and Brodkey [13] and Practuri and Brodkey [14] showed that the sublayer is passive in its reaction to the penetration of coherent structures from the turbulent boundary layer. This passive nature originates from the viscous forces that break the movement of coherent structures. The coherent structures are formed at the interface of the sublayer and turbulent boundary layer.

Within the turbulent boundary layer two flow types can be distinguished: the turbulence generation region and the outer region. The coherent structures formed in the generation region penetrate into the sublayer and into the outer region of the turbulent boundary layer. The stochastic penetration into the sublayer causes a stochastic reduction of sublayer thickness, leading to an increasing air friction and yarn force. The variations in yarn force found, can therefore be explained by the stochastic penetration of coherent structures into the sublayer. This model of the turbulent boundary layer has been used by van Dongen *et al.* [15] to predict the fluxes of heat and momentum at the wall of a flat plate.

The spinning filament forms a small diameter cylinder the sublayer of which has not been investigated visually. According to equation (11) the difference in shear stress between the sublayer and the boundary layer will increase with decreasing cylinder diameter. For small diameter cylinders the penetration of coherent structures from the boundary layer into the sublayer is more hindered by viscous dissipation and by the necessity of acceleration during penetration than in the case of a large diameter cylinder. So, the sublayer flow of a small diameter cylinder will have a more laminar character than that of a large diameter cylinder.

In this paper the sublayer flow is therefore described as a laminar flow, although the variation found in the yarn forces measured can only be explained from coherent structures disturbing the sublayer flow. The sublayer flow will probably not have a fully laminar character, but the frequency and intensity of the disturbances are supposed to be so low that as compared with the viscous transport, the transport of momentum in the sublayer as a result of turbulence can be neglected.

4.4. *Theoretical equations for the velocity profile and thickness of the sublayer*

The velocity profile in the laminar viscous sublayer can be calculated from the dominance of the viscous forces and from the absence of acceleration of the fluid. The viscous forces on cylinders concentric with the filament surface are equal. This is expressed by the supposition that the value of K in the following equation will be independent of the radial distance r

$$\eta_a r \frac{dv_a}{dr} = K. \tag{11}$$

The value of K is directly connected with the value of *Bm*, using equation (5) and the definition of τ_w, which leads to

$$\tau_w = \frac{K}{R} = -\eta_a \frac{v}{R} Bm. \tag{12}$$

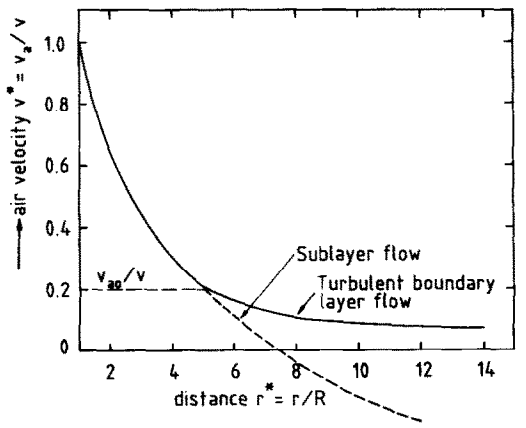

FIG. 4. Calculated velocity profiles in sublayer (equation (14)) and turbulent layer [7] of a spinning filament ($\phi_m = 2.67 \times 10^{-5}$ kg s^{-1}; $v = 50$ m s^{-1}; $Re_R = 33$; $Bm = 0.40$).

From equation (12) K is eliminated and the resulting equation is integrated.

The new integration constant found follows from the extra boundary condition

$$v = v_a \quad \text{for } r = R. \tag{13}$$

This results in the following velocity distribution of the air flow in the sublayer:

$$\frac{v_a}{v} - 1 = -Bm \ln\left(\frac{r}{R}\right). \tag{14}$$

For a laminar boundary layer Sakaidis [16] found the same velocity distribution as we found for the sublayer next to the turbulent boundary layer. He also used the same definition for Bm. This logarithmic velocity profile, outside the cylinder, is formed in a way comparable with that of the parabolic velocity profile for the viscous flow inside a cylindrical pipe (Poiseuille flow). In a turbulent boundary layer flow logarithmic profiles are often found, e.g. equation (3.1.14) in ref. [8]. According to the graphical representation of equation (14) in Fig. 4 the velocity profile will become negative for large r^* values. This is unrealistic. To get an impression of the real velocity profile, the turbulent boundary layer calculations of Sparrow *et al.* [7] have been applied, resulting in the velocity profile shown in Fig. 4.

The sublayer will extend no further than the point where the velocity profile deviates from the sublayer velocity profile.

The sublayer will have a thickness originating from the penetration depth of the coherent structures from the turbulent boundary flow into the sublayer. The interaction can be characterized by the relative velocity drop P across the sublayer defined by the air speed v_{a0} at the transition of the sublayer and the turbulent boundary layer and by

$$P = (v - v_{a0})/v. \tag{15}$$

According to Fig. 4 the P values will be 0.78. Because of the approximations used the P value may vary from 0.7 to 1.0.

The thickness of the sublayer δ is connected with the relative velocity drop P and the velocity distribution in the sublayer by equation (14). Elimination of v_{a0} from this equation and equation (15) results in

$$Bm = P(\ln(1+\delta/R))^{-1}. \tag{16}$$

This equation indicates that the effect of the air friction on the spinning filament is closely related to the thickness of the viscous sublayer, on the assumption that the relative velocity drop P across the sublayer has a constant value. After solidification of the yarn, the turbulent boundary layer has been fully developed and therefore a constant value of P seems realistic.

All parameters affecting the sublayer thickness interact in such a way that relationships can be obtained between dimensionless quantities. The parameters influencing the Bingham number are: the distance x, the spinning speed v and the output ϕ_m. The output combined with the spinning speed determine the yarn radius R. From these parameters the following dimensionless numbers can be derived: δ/R, x/R and $Re_x = v\,x/v_a$. A power-law relation between these dimensionless numbers has the following form:

$$\delta/R = A(x/R)^{\alpha} Re_x^{\beta}. \tag{17}$$

The influence of the distance x on Bm can be found by substituting equation (17) into equation (16)

$$Bm = P(\ln(1 + A(x/R)^{\alpha} Re_x^{\beta}))^{-1}. \tag{18}$$

This relationship expresses in dimensionless form the experimentally found influences of x, R and v on the Bingham number.

The reasoning of Prandtl [9] for explaining the similarity of thermal and dynamical transfer for pipe flow, applies equally to the sublayer flow. According to the comparison of heat transfer and fluid friction of Colburn mentioned by Jacob (Section (24.6) in ref. [5]) then

$$Nu = Bm\, Pr^{1/3}. \tag{19}$$

By substituting equation (18) into equation (19) a sublayer expression for the heat transfer is reached.

As the thickness of the sublayer is very small in absolute value, the velocity distribution in the sublayer cannot easily be measured. The measuring spot of a laser Doppler anemometer will be too large. The sublayer around the hot wire of a hot wire anemometer will strongly interact with the sublayer of the thin filament. The sublayer model can also be checked by comparing equations (18) and (19) with experimental results for different situations.

5. FITTING OF THE EXPERIMENTAL RESULTS INTO THE SUBLAYER MODEL

5.1. *Introduction*

In order to fit all experimental results into the sublayer model a series of successive steps are used.

(1) From our measurements on spinning yarn, values of A, α and β are calculated, while the P value of 0.8 is estimated from the velocity profile of the sublayer flow.

(2) The experimental results from hot wires are used here to determine the values of A, α and β on the assumption that $P = 1.0$. For very small diameter cylinders, the boundary layer flow becomes laminar and the P value has to be 1.0, independent of the flow direction. Heat transfer of hot wires applied in hot wire anemometers, is used here. Hot wires are the smallest diameter cylinders for which accurate results are known. In this case the flow direction is transverse to the wire.

(3) Experimental results for heat transfer due to a longitudinal turbulent flow on a cylinder of 7.7 mm diameter are fitted to the relation found from measurements on the hot wires by adapting only the value of P.

(4) The experimental results for spinning yarn can also be fitted to the relation found for hot wires by adapting only the P value. In Figs. 7 and 8 the results are illustrated.

5.2. *Fitting of our results from spinning yarn*

From the experimentally found values of the Bingham numbers in Table 1 the sublayer thickness can be calculated by using equations (16) and (1) and $P = 0.8$. This value of P is in accordance with Fig. 4, although the choice as such is arbitrary. For larger P, the calculated sublayer thickness will be larger. In Table 1 and Figs. 5 and 6 the resulting values of the sublayer thickness are given. From these data various relationships can be found by power-law regression for the influence of output per hole and spinning speed. They are all of the shape

$$\delta = Bv^{b_1}\phi_m^{b_2}. \tag{20}$$

This experimental relation must coincide with the dimensionless relation (17) for δ, thus leading to

$$\alpha = 1-2b_2 \quad \text{and} \quad \beta = b_1+b_2. \tag{21}$$

Due to the large scatter in experimental values of Bm, more values for the parameter set A, α and β are possible, all fitting with the data of Table 1. The influence of distance x expressed by equation (9) must coincide, too. This results in an extra value for $(\alpha+\beta)$, which is used to improve the approximations of α and β.

The influence of distance x can easily be calculated from the derivative dBm/dx using equation (18). After rearranging, it follows that:

$$\frac{d}{dx}Bm = \frac{-Bm^2}{P}\,\frac{\delta/R}{1+\delta/R}\,\frac{\alpha+\beta}{x} = -Bm^2\frac{(\alpha+\beta)}{x}. \tag{22}$$

The neglect in the last part of this equation is justified by the value of $\delta/R = 5$ in Fig. 4. By integration it follows:

$$Bm(1.6)-Bm(4.4) = (\alpha+\beta)Bm^2(3.0)\ln(4.4/1.6). \tag{23}$$

It is found from equation (9) that

$$Bm(1.6)-Bm(4.4) = 0.062.$$

Taking a value for $Bm(4.4)$ in the middle of the range of experimental values shown in Fig. 2, the value of $Bm(3.0)$ is calculated. Hence

$$Bm(3.0) = Bm(4.4)-\tfrac{1}{2}(Bm(1.6)-Bm(4.4)) = 0.37.$$

Equation (23) yields: $\alpha+\beta = 0.45$.

The three experimental values of b_1, b_2 and $(\alpha+\beta)$ determine the two values of α and β, which results in an improved fit. From the systematic investigation into the influence of the output it follows (Fig. 6): $b_2 = 0.18$. In this set-up three settings are repeated. Two duplicates do not fit in this systematic investigation (Fig. 6) and it can also be supposed that the influence of the output is negligible or $b_2 = 0$. Both possibilities will be worked out.

Suppose there is a slight influence of the output on the sublayer thickness. The following values are found:

$$b_1 = -0.75; \quad b_2 = -0.18 \quad \text{and} \quad \alpha+\beta = 0.45.$$

From equation (21) it follows:

$$\alpha = 1.36; \quad \beta = -0.93 \quad \text{and} \quad \alpha+\beta = 0.43.$$

All experimental influences correspond with these values of α and β.

If the influence of the output on the sublayer thick-

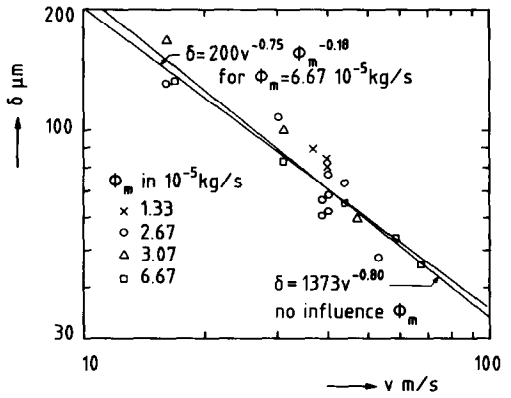

FIG. 5. Influence of the yarn speed on the sublayer thickness for various outputs per orifice.

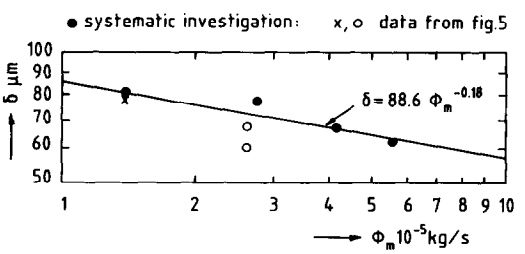

FIG. 6. Influence of the output per orifice on the sublayer thickness for $v = 40$ m s^{-1}.

ness is neglected, then with $b_2 = 0$ regression of the data from Table 1 gives $b_1 = -0.80$. This yields

$$\alpha = 1; \beta = -0.80 \quad \text{and} \quad \alpha+\beta = 0.20.$$

This last value does not fit with the experimentally found influence of distance x, which led to $\alpha+\beta = 0.45$.

If an average value $\alpha+\beta = 0.33$ is taken, it follows with $b_2 = 0$ that

$$\alpha = 1; \quad \beta = -0.67.$$

The correlations of both possible fits with the experimental data are equally acceptable. Both fits have in common that the value of $(\alpha+\beta)/\alpha = 1/3$. This common feature can be used for changing equation (18) into

$$Bm = P \ln (1 + a_1 (Re_x/Re_R^3)^{a_2})^{-1}. \qquad (24)$$

Regression of all data of Table 1 results in $a_1 = 0.56$ and $a_2 = 0.41$, the coefficient of correlation being 0.96.

Neglecting the influence of the outputs: $a_1 = 0.77$ and $a_2 = 0.33$ with a coefficient of correlation of 0.95.

It can be concluded that the experimentally determined influences on the air friction are fully described by equation (24) with $P = 0.8$ and by the values of the parameters mentioned here. That the influence of distance x, output and spinning speed coincides with the experimentally found influences, strengthens the credibility of this approximation. However, the choice of P still has to be improved.

5.3. *Hot wire anemometer results*

In the previous part P has arbitrarily been chosen to be 0.8. For very small diameter cylinders P will be 1.0. It is supposed that $P = 1.0$ for the transverse flow along a hot wire having diameters over 5 μm and Reynolds numbers ranging from 2 to 100. As the thickness of the sublayer is of the order of 100 μm, the sublayer will be much thicker than the diameter of the hot wire. Only the sublayer behaviour will be decisive for transfer of heat. Sandborn and Laurence [17] and Davies and Fischer [18] have performed accurate measurements on the heat transfer from hot wires. The Nusselt numbers, Nu, found relate to the Bingham number, Bm, using equation (19). From these results for hot wires it follows that $a_1 = 1.29$ and $a_2 = 0.33$. All data mentioned can be described by

$$Bm = P(\ln (1 + 1.29 Re_x^{1/3} Re_R^{-1}))^{-1}. \qquad (25)$$

The correlation of the data with this analytical expression is sufficient, according to Fig. 7. For this correlation of data P is supposed to be 1.0.

5.4. *Results for spinning yarn*

All results for spinning yarn can also be fitted to equation (25) by adapting the parameter value of P (see Fig. 8).

Our experiments on a spinning yarn yield the value $P = 1.0$. The turbulent boundary layer calculations

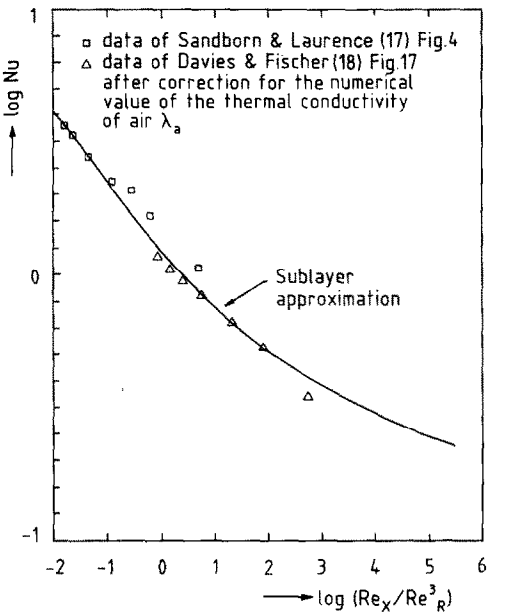

FIG. 7. Comparison of equations (25) and (19) with experimental results on heat transfer of hot wire anemometers.

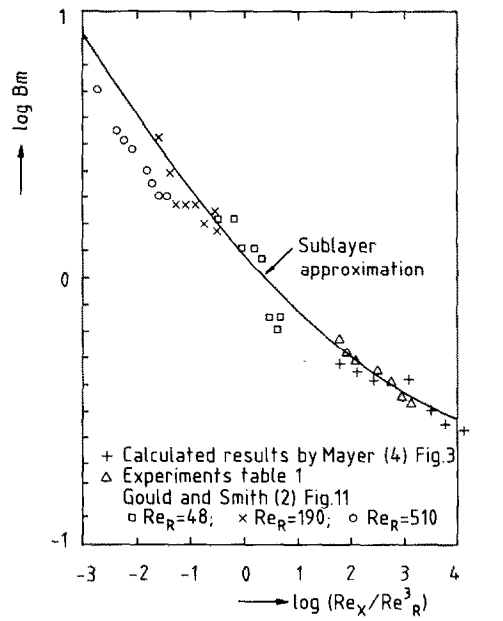

FIG. 8. Comparison of equation (25) with results for air friction on spinning filaments.

made by Mayer also result in data fitting to this relationship for $P = 1.0$.

The experimental results of Gould and Smith in Fig. 11 of ref. [2] are rearranged to values for Bm and (Re_x/Re_R^3). The experiments of Gould and Smith correlate well with equation (25) for $P = 0.92$. This difference in P can be explained from the larger cylinder diameters used by Gould and Smith in their experiments. They used (Re_x/Re_R^3) values ranging from 10^{-3} to 4 and filament diameters from 75 to 100 μm. Our experiments were carried out at (Re_x/Re_R^3)

values ranging from 50 to 1000 and filament diameters from 20 to 60 μm.

5.5. *Results for heated tubes*

Equation (25) has also been correlated with experimental results for heat transfer to air by a cylinder with a diameter of 7.75 mm. Adomaitis *et al.* [19] determined Nu_x for this cylinder at $Re_x = 10^6$ and found $Nu_x = 1600$ (see Fig. 5 of ref. [19]). According to Fig. 2 of ref. [19] the value $x/R = 42$ for $Re_x = 10^6$; so $Re_R = 24\,000$. Substitution of these data into equation (25) gives $Bm = 185P$. From equation (19) and $Nu_x = (x/R)Nu_R$ it follows $Nu_x = 8630P$. The experimental results of Adomaitis *et al.* correlate with equation (25) for $P = 0.23$. This low P value can be explained from the large diameter of the cylinder used. For the experiments made by Adomaitis *et al.* the value of (Re_x/Re_R^3) is 10^{-7}. This value differs strongly from the situation with hot wires and spinning yarn. It seems that equation (25) can be used to correlate experimental data also for cylinders with a larger diameter of several millimetres.

5.6. *Conclusion*

It has been found possible to correlate various experimental data for transfer of heat and momentum with equation (25).

The velocity drop P across the sublayer proves to depend on the diameter of the cylinder. For diameters ranging from 5 to 40 μm, $P = 1.0$. For diameters of 90 μm, $P = 0.92$. For a diameter of 7.5 mm, $P = 0.23$.

6. DISCUSSION

As all heat flowing through the turbulent boundary layer must first travel through the sublayer, the sublayer behaviour will influence the transport in both layers. For turbulent boundary layer calculations use is normally made of the velocity profile of the sublayer. It may be possible to simplify the turbulent boundary layer calculations by making use of equations (25) and (17), derived here from the sublayer concept.

The experimental results for the air friction on spinning yarn can be explained also from a turbulent boundary layer description. The turbulent boundary layer calculation, however, requires a complex numerical procedure, limiting general use. From the sublayer concept an analytical expression is found which can be applied more easily to model calculations for simulating the process of melt spinning.

Different physical models are used for the calculations based on the sublayer concept or the turbulent boundary layer concept. As the total flow through both layers must be equal, the result of both calculations should be equal. Because of the simplicity of the physical model for the sublayer, the use of the sublayer concept is advantageous especially for small diameter cylinders.

The sublayer is a purely viscous layer, reacting passively to coherent turbulent structures penetrating from the boundary layer into the sublayer. The motion of these coherent structures is broken by viscous forces and deceleration. If the filament diameter is very small, the full velocity drop takes place across the sublayer thickness, which is expressed by $P = 1$. The sublayer thickness can be expressed by a dimensionless relationship (see equation (17)). The results of experiments on filaments with diameters under 20 μm can be explained with $P = 1$ and the following relation:

$$\delta/R = 1.29(x/R)Re_x^{-2/3}. \tag{26}$$

According to equation (26) the sublayer thickness will be independent of filament radius R and depend only on distance x and Re_x. This experimental result suggests that the sublayer thickness is solely determined by the velocity drop across the sublayer and the distance x.

Acknowledgements—I would like to thank G. Dubbeldam and H. Oesterholt for their help in performing the experiments and the Enka Company for their permission to publish this work. The contribution of Mr Bezemer in reading the manuscript is especially acknowledged.

REFERENCES

1. A. Ziabicki, *Fundamentals of Fiber Formation*. Wiley, New York (1974).
2. J. Gould and F. S. Smith, Air-drag on synthetic textile monofilaments and yarns in axial flow at speeds of up to 100 m s^{-1}, *J. Text. Inst.* **71**, 38–59 (1980).
3. J. R. Glicksman, The cooling of glass fibers, *Glass Technol.* **9**(5), 131–138 (1968).
4. M. Mayer, Berechnung von Schubspannung und Wärmeübergang an längsgeströmten Fäden, *Chemie-Ingr-Tech.* **42**(6), 396–402 (1970).
5. M. Jacob, *Heat Transfer*, Vol. 1. Wiley, New York (1949).
6. D. Acierno, J. N. Dalton, J. M. Rodrigues and J. L. White, Rheological and heat transfer aspects of the melt spinning of monofilament fibers of polyethylene and polystyrene, *J. Appl. Polym. Sci.* **15**, 2395–2415 (1971).
7. E. M. Sparrow, E. R. G. Eckert and W. J. Minkowycz, Heat transfer and skin friction for turbulent boundary layer flow longitudinal to a circular cylinder, *J. Appl. Mech.* 37–43 (March 1963).
8. A. Walz, *Strömungs- und Temperaturgrenzschichten*. G. Braun, Karlsruhe (1966).
9. L. Prandtl, Eine Beziehung zwischen Wärmeaustausch und Strömungswiderstand der Flüssigkeiten, *Phys. Z.* **XI**, 1072–1078 (1910).
10. I. Tani, History of boundary layer theory, *Ann. Rev. Fluid Mech.* **9**, 87–111 (1977).
11. H. A. Einstein and J. Li, The viscous sublayer along a smooth boundary, *J. Engng Mech. Div. Am. Soc. Civ. Engrs* **82**(EM 2), 945 (1956).
12. S. J. Kline, W. C. Reynolds, F. A. Schraub and P. W. Rundstadler, The structure of turbulent boundary layers, *J. Fluid Mech.* **30**, 741–773 (1967).
13. E. R. Corino and R. S. Brodkey, A visual investigation of the wall region in turbulent flow, *J. Fluid Mech.* **37**(1), 1–30 (1969).
14. A. K. Practuri and R. S. Brodkey, A stereoscopic visual study of coherent structures in turbulent shear flow, *J. Fluid Mech.* **89**(2), 251–272 (1978).
15. F. G. van Dongen, A. C. M. Beljaars and D. A. de Vries,

A periodic intermittent model for the wall region of a turbulent boundary layer, *Int. J. Heat Mass Transfer* **21,** 1099–1109 (1978).
16. B. C. Sakaidis, Boundary-layer behaviour on continuous solid surfaces: parts I, II, III, *A.I.Ch.E. Jl* 26–28, 221–225, 467–472 (1961).
17. V. A. Sandborn and J. C. Laurence, Heat loss from yawed hot wires at subsonic Mach numbers, NACA Techn. Note No. 3563 (1955).
18. P. O. A. L. Davies and M. J. Fischer, Heat transfer from electrically heated cylinders, *Proc. R. Soc.* **A280**(1383), 486–527 (1964).
19. J. E. J. Adomaitis, B. A. Česna and J. V. Vilemas, Experimental study of heat transfer and friction on a cylinder in longitudinal turbulent flow of air with variable physical properties, *Heat Transfer—Sov. Res.* **15,** 52–74 (1983).

DESCRIPTION DE SOUS-COUCHE POUR LE FROTTEMENT D'AIR AGISSANT SUR DES FILAMENTS FINS PENDANT LE TREFILAGE

Résumé—Le frottement de l'air sur des filaments de petit diamètre est explique à partir d'une description de sous-couche d'air le long de la surface du filament. Le frottement d'air sur le filament est exprimé sans dimension par le nombre de Bingham *Bm*

$$Bm = P[\ln(1+1{,}29Re_x^{1/3}\,Re_R^{-1})]^{-1}$$

où *P* est une mesure de la perte de vitesse relative à travers la sous-couche. Des calculs à partir de cette formule correspondent à de nombreux résultats expérimentaux et à un calcul de couche limite turbulente. Cette formule explique aussi des résultats expérimentaux de transfert thermique obtenus avec des fils chauds d'anémométrie et avec des cylindres dans un écoulement longitudinal.

BESCHREIBUNG DER LUFTREIBUNG AN DÜNNEN FÄDEN WÄHREND DES SCHMELZSPINNENS MIT HILFE EINER STRÖMUNGS-UNTERSCHICHT

Zusammenfassung—Die Luftreibung an Fäden mit kleinem Durchmesser wird durch Betrachtung einer Strömungs-Unterschicht entlang der Fadenoberfläche erklärt. Zur Beschreibung dient die dimensionslose Bingham-Zahl

$$Bm = P(\ln(1+1{,}29Re_x^{1/3}\,Re_R^{-1}))^{-1}$$

wobei *P* ein Maß für die relative Geschwindigkeitsabnahme in der Unterschicht ist. Die mit dieser Formel berechneten Ergebnisse stimmen mit vielen experimentellen Ergebnissen und mit einer turbulenten Grenzschicht-Rechnung überein. Die Gleichung erklärt auch experimentelle Ergebnisse, die für die Wärmeübertragung an Hitzdrähten in Anemometern und an längs angeströmten Zylindern ermittelt worden sind.

МОДЕЛЬ ПОДСЛОЯ ДЛЯ УЧЕТА ВЛИЯНИЯ ТРЕНИЯ ВОЗДУХА ПРИ ВЫТЯГИВАНИИ ТОНКИХ НИТЕЙ ИЗ РАСПЛАВА

Аннотация—Влияние трения воздуха на нити малого диаметра объясняется с помощью модели подслоя для потока воздуха вдоль поверхности нити. Трение воздуха на нитях можно определить, используя безразмерное число Бингама

$$Bm = P(\ln(1+1{,}29Re_x^{1/3}\,Re_R^{-1}))^{-1}$$

где *P*—мера относительного уменьшения скорости поперек подслоя. Полученные с помощью данной формулы результаты согласуются с многочисленными экспериментальными данными и с расчетом турбулентного пограничного слоя. Эта формула также позволяет объяснить экспериментальные данные по теплообмену, которые были получены с использованием термоанемометра и цилиндров при продольном обтекании.